ACS Applied Materials & Interfaces
DOI: 10.1021/acsami.8b12596

Versatile and scalable strategy to grow sol-gel derived 2H−MoS_2 thin films with superior electronic properties: a memristive case.

Journal:	*ACS Applied Materials & Interfaces*
Manuscript ID	Draft
Manuscript Type:	Article
Date Submitted by the Author:	n/a
Complete List of Authors:	Nardi, Marco V.; University of Trento, Department of Industrial Engineering Timpel, Melanie; University of Trento, Department of Industrial Engineering Ligorio, Giovanni; Humboldt-Universität zu Berlin, Institut für Physik Zorn Morales, Nicolas; Humboldt-Universität zu Berlin, Institut für Physik Chiappini, Andrea; Istituto di Fotonica e Nanotecnologie Consiglio Nazionale delle Ricerche Toccoli, Tullio; Istituto dei Materiali per l'Elettronica ed il Magnetismo Sezione di Trento Consiglio Nazionale delle Ricerche, Verucchi, Roberto; Istituto dei Materiali per l'Elettronica ed il Magnetismo IMEM-CNR, Ceccato, Riccardo; University of Trento, Department of Industrial Engineering Pasquali, Luca; Dipartimento di Ingegneria dei Materiali e dell'Ambiente, List-Kratochvil, Emil; Humboldt-Universität zu Berlin, Institut für Physik Quaranta, Alberto; University of Trento, Industrial Engineering Dirè, Sandra; University of Trento, Department of Industrial Engineering

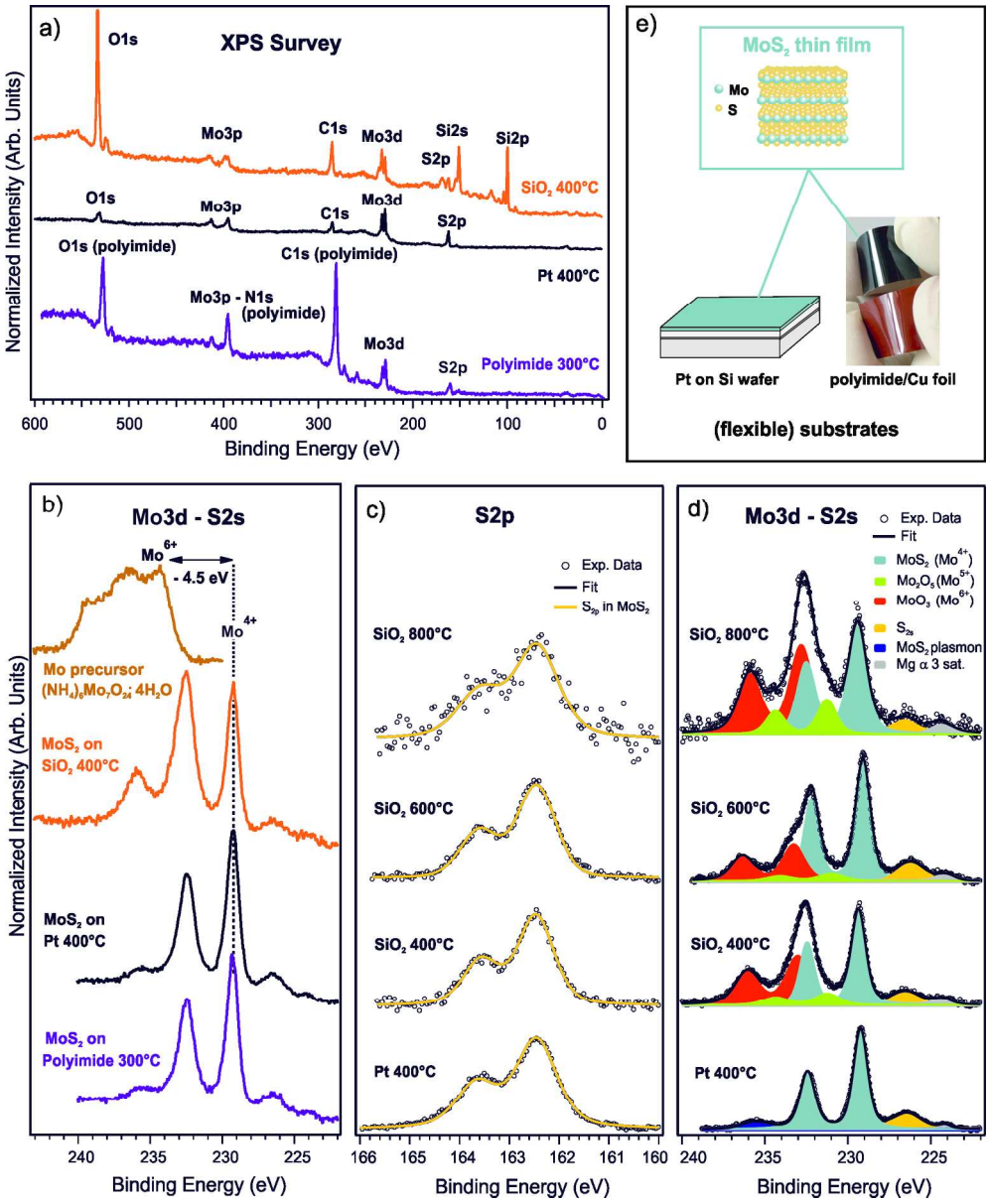

Figure 1. (a) XPS survey spectra of spin coated films on different substrates (polyimide, Pt and SiO_2) annealed at low temperature (T = 300/400°C); (b) Mo 3d + S 2s core level XPS spectra of Mo precursor and spin coated films annealed at low temperature; (c) S 2p and (d) fitted Mo 3d + S 2s core level XPS spectra of spin coated films on Pt and SiO_2 substrates annealed at different temperatures (T = 400 – 800°C); (e) schematic summary of the XPS findings: MoS_2 thin films without any additional oxidized Mo species were formed on Pt and polyimide substrates (upper substrate in the photograph corresponds to the MoS_2 film on polyimide/Cu foil, whereas the lower one is untreated).

177x215mm (300 x 300 DPI)

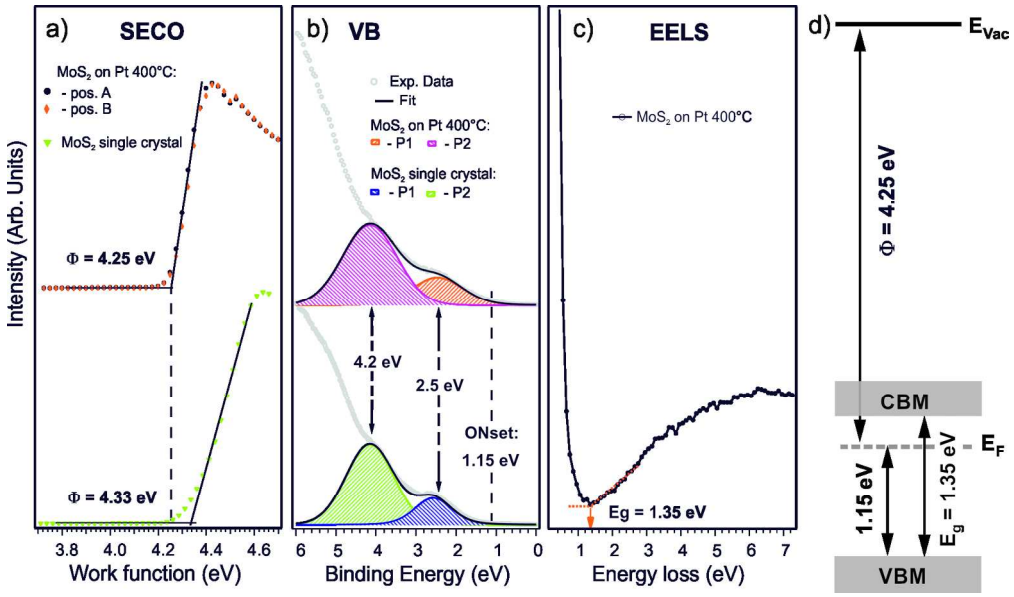

Figure 2. (a) Secondary electron cutoff (SECO) and (b) valence band (VB) region UPS spectra of the sol-gel derived MoS_2 thin film on Pt (annealed in Ar at 400 °C) compared to the spectra of a MoS_2 reference (single crystal); (c) EELS spectrum of the sol-gel derived MoS_2 thin film on Pt; (d) corresponding energy-level diagram. The energetic positions of the E_{vac} and VBM relative to the Fermi level E_F were determined by UPS measurements, whereas the energy gap E_g was derived by EELS.

170x100mm (300 x 300 DPI)

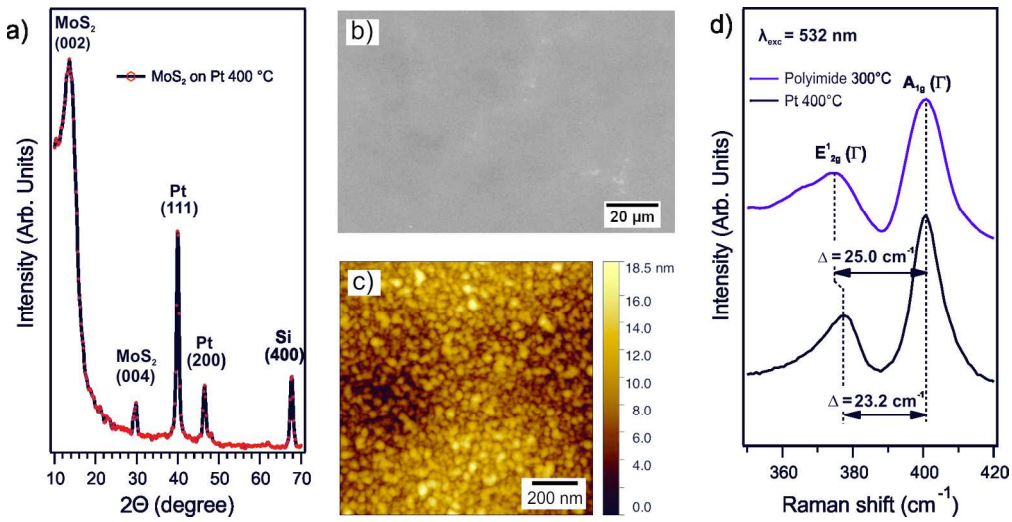

Figure 3. (a) XRD spectrum, (b) SEM image, and c) AFM height image of the sol-gel derived MoS_2 thin film on Pt substrate (annealed in Ar at 400 °C). (d) Non-resonant Raman spectra (λ = 532 nm) of the sol-gel derived MoS_2 thin film on Pt and polyimide substrate. The spectral distance between the $E^1_{2g}(\Gamma)$ and the $A_{1g}(\Gamma)$ Raman modes is given by the vertical dashed lines.

167x85mm (300 x 300 DPI)

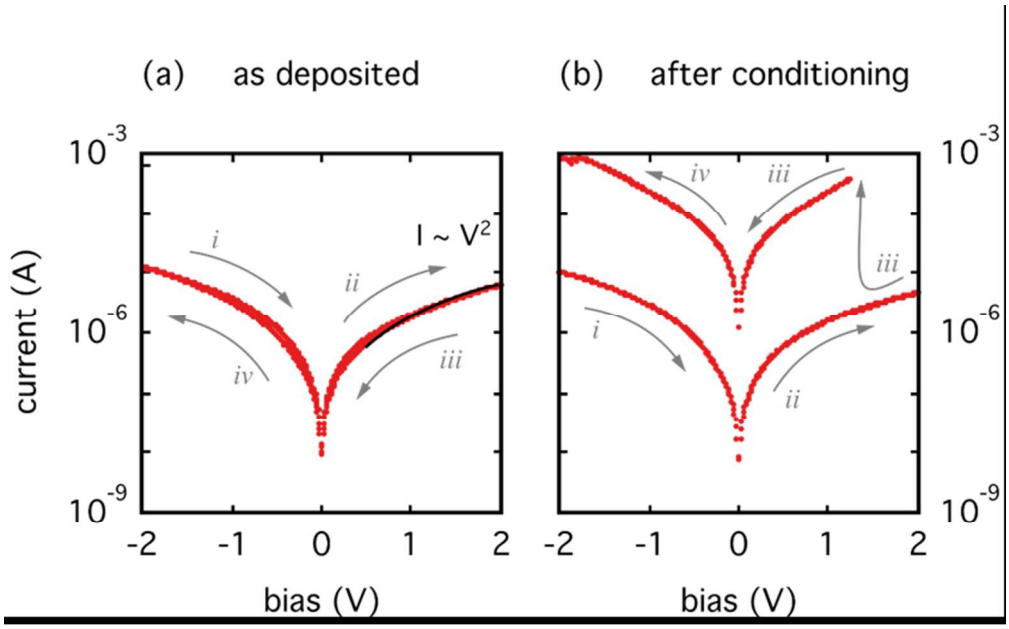

Figure 4. I-V curve measurements performed with a probe station of MoS_2 film grown on Pt. The film was first measured as deposited (a) and then conditioned (b) through sweep cycles (the solid black line represents a guide for the eye indicating a quadratic dependency for I from V). Upon conditioning the film displays a resistive switch from a high to a low state (b). The arrow indicates the voltage sweep progression during I-V measurements.

141x87mm (150 x 150 DPI)

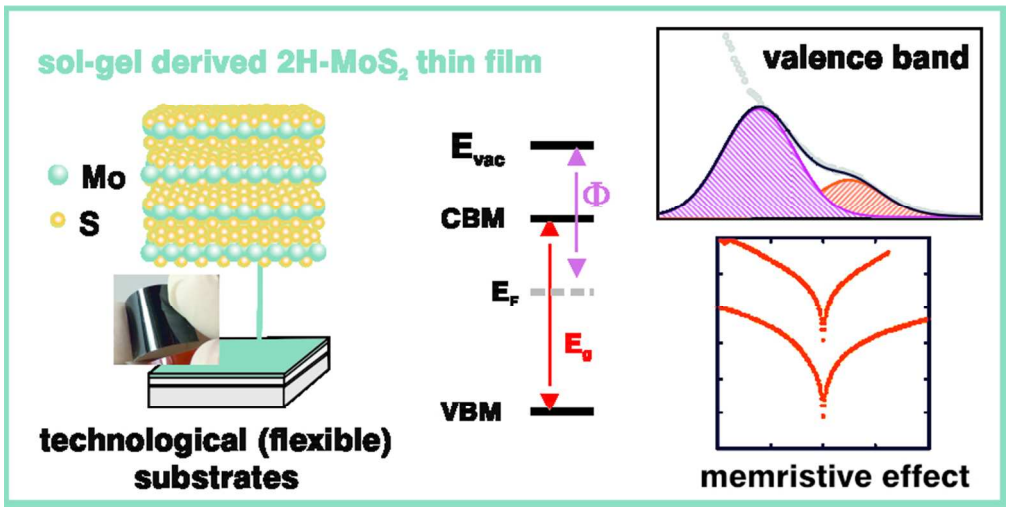

Table of Contents Graphic

80x40mm (300 x 300 DPI)

Versatile and scalable strategy to grow sol-gel derived 2H−MoS_2 thin films with superior electronic properties: a memristive case.

Marco V. Nardi[1,Δ,], Melanie Timpel[1,Δ,*], Giovanni Ligorio[2], Nicolas Zorn Morales[2], Andrea Chiappini[3], Tullio Toccolli[4], Roberto Verucchi[4], Riccardo Ceccato[1], Luca Pasquali[5,6,7], Emil J.W. List-Kratochvil[2], Alberto Quaranta[1] and Sandra Dirè[1]*

[1]Department of Industrial Engineering, University of Trento, Via Sommarive 9 – 38123 Trento, Italy. E-mail: marcovittorio.nardi@unitn.it, melanie.timpel@unitn.it

[2]Institut für Physik, Institut für Chemie & IRIS Adlershof, Humboldt-Universität zu Berlin, Brook-Taylor Straße 6 – 12489 Berlin, Germany.

[3]CNR-IFN, CSMFO Lab., Via Alla Cascata 56/C – 38123 Trento, Italy.

[4]Istituto dei Materiali per l'Elettronica ed il Magnetismo, IMEM-CNR, Sezione di Trento, Via alla Cascata 56/C, Povo – 38100 Trento, Italy.

[5]IOM-CNR Institute, Area Science Park, SS 14 Km, 163.5 – 34149 Basovizza, Trieste, Italy.

[6]University of Modena e Reggio Emilia, Engineering Department, "E. Ferrari", Via Vigolese 905 – 41125 Modena, Italy.

[7]Department of Physics, University of Johannesburg, PO Box 524, Auckland Park, 2006, South Africa.

KEYWORDS. MoS_2 thin film; sol-gel synthesis; photoelectron spectroscopy; memristor device

ABSTRACT

Transition metal dichalcogenides, such as molybdenum disulfide (MoS_2), show peculiar chemical/physical properties that enables their use in applications ranging from micro- and nano-optoelectronics to surface catalysis, gas and light detection and energy harvesting/production. One main limitation to fully harness the potential of MoS_2 is given by the lack of scalable and low environmental impact synthesis of MoS_2 films with high uniformity, hence setting a significant challenge for industrial applications. In this work, we develop a versatile and scalable sol-gel derived MoS_2 film fabrication by spin coating deposition of an aqueous sol on different technologically relevant, flexible substrates with annealing at low temperatures (300°C) and without the need of sulfurization and/or supply of hydrogen as compared to cutting-edge techniques. The electronic and physical properties of the MoS_2 thin films were extensively investigated by means of surface spectroscopy and structural characterization techniques. The potential use of sol-gel grown MoS_2 as candidate material for electronic applications was tested via electrical characterization and demonstrated via the reversible switching in resistivity typical for memristors. The obtained results highlight that the novel low-cost fabrication method has a great potential to promote the use of high-quality MoS_2 in technological and industrial relevant scalable applications.

1. INTRODUCTION

Transition metal dichalcogenides (TMDs), and in particular molybdenum disulfide MoS_2, attracted interest in the past decade in both the scientific and the industrial community due to their peculiar properties such as the tunable and layer-dependent band gap, mechanical properties, piezoelectric effect,[1] strong light absorption, etc.[1–4] The layered structure and the weak van der Waals interactions[5–7] between the individual layers are of prominent importance for industrial applications such as dry lubricants able to withstand high temperatures[8] and catalytic properties used for example in the petrochemical industry, which can easily be tuned via selective interlayer doping.[9,10] Within the TMDs, MoS_2 shows interesting properties, for instance, depending on the crystal structure and the sulfur S atom arrangements, different polymorphisms can be found. In particular, two phases of MoS_2 are of prominent importance, namely the bulk 2H phase and the 1T phase.[11,12] The 1T phase is metastable and shows metallic character, whereas the bulk 2H phase exhibits semiconducting behavior with n-type character and an indirect band gap of 1.3 eV.[13,14] Single 2D type layers of 2H−MoS_2 exhibit a direct band gap of 1.8 eV,[13] a n-type character of the semiconductor and a rich photophysics of excitonic exited states, while an increasing number of layers yields an indirect band gap material.[15] These properties together with mechanical flexibility, good optical transmittance and high charge carrier mobility makes MoS_2 an excellent candidate for electronics and optoelectronics devices.[16–18]

Beyond the use as few- or single-layered structure in electronic applications,[19,20] MoS_2 thin films[21] were recently used in a wide variety of applications ranging from water splitting related to its surface catalytic properties,[22] to charge transportation layers in energy storage devices like lithium ion batteries,[23] conversion devices and high-end electronic apparatus,[24,25] Q-switched laser[26] and electro-catalytic applications[27] as well as multilayer structures in field effect

transistors.[28] Among the large number of techniques recently developed to synthetize thin films and single/few layer structures of MoS_2, a versatile and industrially scalable one for large-scale production of MoS_2 films is still lacking in literature.

Recent developments in methods to grow MoS_2 thin films based on vapor phase growth,[29,30] as well as solution-based approaches such as the sulfurization of a Mo-containing sol-gel precursor[31] and thermal decomposition[32–38] or agent-induced reduction[35] of spin coated single precursor ammonium thiomolybdate $[(NH_4)_2MoS_4]$ have enabled the production of large-scale MoS_2 films. However, the main drawbacks of these approaches are the need of additional sulfurization steps at high annealing temperatures (~1000°C), and/or reducing atmosphere/agents to achieve highly crystalline and stoichiometric MoS_2 films. The requirement of such high temperatures for the annealing treatment clearly inhibits the employment in industrially scalable-application; despite some recent efforts using lower temperatures that are compatible with technologically relevant substrates,[35,36,39] such as polyimide, polybenzimidazole, polyetheretherketone, cellulose, carbon paper and cotton thread, there is still a demand of lower temperature treatments enabling the growth of crystalline MoS_2 films with good electronic properties.

To obtain large-area high-quality MoS_2 thin films, we adopted a facile water-based sol-gel route, which was previously used to synthesize MoS_2 nanopowders.[40,41] More specifically, ammonium molybdate tetrahydrate $[(NH_4)_6Mo_7O_{24}\cdot 4H_2O]$ was used as Mo source and thioacetamide (CH_3CSNH_2) as S source, which are stabilized in solution by the chelating agent pentaacetic acid (DTPA).[41] For the MoS_2 thin film formation developed herein, the as-prepared sol-gel precursor was spin coated onto technologically relevant substrates, namely on SiO_2, Pt (grown on a Si wafer) and polyimide, followed by subsequent annealing in Ar atmosphere at low-temperatures (300 – 400°C). A broad spectrum of characterization tools were adopted to validate the quality of the

MoS_2 thin films and its excellent electronic properties that are comparable to that of a MoS_2 single crystal. Furthermore, the role of oxide-containing substrates, such as SiO_2, in oxidizing as-deposited precursors during annealing was investigated by X-ray photoelectron spectroscopy.

Even though this process has been established using spin coating, the deposition of thin films can be still deemed as scalable since the use of the water-based MoS_2 allows the implementation of large-area coating/printing techniques at industrial scale with less impact on the environment than previously developed solution-processed approaches based on organic solvents. Furthermore, for oxide-free substrates it represents a safer synthesis approach without the need of H_2 reducing atmosphere and/or development of toxic byproducts such as H_2S. Due to the low-temperature annealing, desulfurization effects are avoided (i.e., an additional S source during annealing is not needed), and the process is compatible with flexible electronics based on polymeric substrates. The high quality of the sol-gel derived MoS_2 thin film for electronics applications is demonstrated on a memristive device.

2. EXPERIMENTAL

2.1. SOL-GEL SYNTHESIS OF MoS_2 PRECURSOR SOL

All reagents were purchased from Sigma Aldrich with analytically pure reagent grade. The preparation of the MoS_2-based aqueous sol was adapted from the previously reported chelation-assisted sol–gel method developed to grow MoS_2 nanopowders.[41] The schematic illustration of the molecular structures and the chemical reactions are shown in Figure S1 (Supporting Information). Ammonium molybdate tetrahydrate [$(NH_4)_6Mo_7O_{24}\cdot 4H_2O$] (0.2 g, 0.016 mmol) was dissolved in 8 ml of deionized water at room temperature (RT) under continuous stirring. Thioacetamide (CH_3CSNH_2) (0.4 g, 5.32 mmol) was then added to the aqueous solution as S source.

To the light blue resulting solution (solution labelled as A in Figure S1, Supporting Information), 0.05 g of diethylenetriamine pentaacetic acid (DTPA) was added as chelating agent, which turned the solution into dark green (B in Figure S1). After 1 h stirring was stopped and the mixture was heated at 60°C, leading to the formation of a bronze sol (C in Figure S1) that within 3–4 hours gradually turned into a dark brown viscous sol (see D in Figure S1).

2.2 THIN FILM FORMATION

In the present work, we studied the MoS_2 thin film formation on three different substrates. SiO_2 and Pt(50 nm)/Ti(5 nm) on 12-inch Si wafers (in the following denoted as SiO_2 and Pt substrates) were used to investigate the difference induced by the presence of oxygen at the interface of the substrate and the consequent formation of Mo oxidized species (Mo^{6+} and Mo^{5+}) during the MoS_2 film formation. The Pt(50 nm)/Ti(5 nm)/Si wafers were prepared as described in Ref.[42] The third substrate was a flexible polyimide film (Kapton®) with a thickness of 100 μm supported by a copper foil to provide rigidity during the deposition step. Prior to the coating process, all sample substrates (2 cm × 2 cm) were cleaned in deionized water and isopropanol by sonication for 5 min each, followed by an UV/ozone treatment for ~20 min.

Our strategy for MoS_2 thin film fabrication consists in two simple steps, namely (*I)* sol deposition and (*II*) low-temperature annealing to remove the organic moieties and promote MoS_2 crystallization ($T = 300 – 400$ °C, as derived from the TG analysis shown in Figure S2a, Supporting Information). For the sol deposition (after 3 − 4h of reaction) the spin-coating technique was adopted. To ensure film uniformity and to optimize fabrication time in the laboratory, the MoS_2 film was achieved through a stepwise procedure:[43] (*i*) acceleration from 0 rpm to 1300 rpm in 2 s,

(*ii*) 2 s at 1300 rpm, (*iii*) acceleration from 1300 rpm to 2000 rpm in 2 s (*iii*) 2s at 2000 rpm, (*iv*) acceleration from 2000 rpm to 3000 rpm in 1s and finally (*v*) 3000 rpm for 49 s. The coatings on Pt and SiO_2 were cured for 5 min in an oven at 60°C, followed by a second layer deposition with the same curing cycle in order to increase the film thickness for characterization of the bulk properties.

Upon MoS_2 deposition, the films were annealed in a tube furnace in Ar atmosphere with a flux of 200 sccm and heating/cooling rate of 4°C/min. Whereas for the coating on Pt only the annealing at 400°C for 4 h was chosen to guarantee the thermal stability of the substrate, the coatings on SiO_2 were annealed at three different temperatures (T = 400, 600 and 800°C) for 4 hours. For the coating on polyimide, only one deposition cycle without heating at 60°C was performed, and the annealing temperature was fixed at 300°C in order to prove the full capability of the deposition process to be used with a wide variety of relevant flexible substrates that typically lose their mechanical properties at temperatures higher than 350 − 400°C.

2.3. CHARACTERIZATION

X-ray photoelectron spectroscopy (XPS) was carried out with a non-monochromatized Mg Kα source (emission line at 1253.6 eV), and ultraviolet photoelectron spectroscopy (UPS) was performed by means of the He I photon at about 21.2 eV. The electron energy analyzer is a VSW HSA100 hemispherical analyzer with PSP electronic power supply and control, the total energy resolution is 0.8 eV for XPS and about 0.1 eV for UPS. The binding energy (BE) scale of XPS spectra was calibrated by using the Au 4f peak at 84.0 eV as a reference, while UPS binding energies were referred to the Fermi level of the same Au clean substrate. The secondary electron cutoff (SECO) spectra were measured with a sample bias of -7.0 V.

Electron energy loss spectroscopy (EELS) was carried out with a Leybold electron gun (EQ22/35) operated at 1000 eV of primary beam energy and a CLAM2 (VG Microtech) electron analyzer, with a resolution of 0.1 eV. Electron beam current on the sample was 2 nA.

X-ray diffraction (XRD) spectra were collected on films with a Rigaku D-Max III diffractometer in glancing incidence configuration, using Cu-Kα radiation and a graphite monochromator in the diffracted beam. Asymmetric scan geometry was adopted in order to enhance the signal stemming from the MoS_2 thin film. Typical measurements were performed in the (2θ) range of $10 - 70°$ with an incidence angle of 1°, sampling interval of 0.05° and counting time of 8 s.

Scanning electron microscopy (SEM) images were obtained using a JSM-5500 scanning electron microscope (JEOL technics Ltd.) with acceleration voltage of 10 kV.

The atomic force microscopy (AFM) images were acquired by a commercially available Dimension Icon AFM from Bruker in PeakForce Tapping mode. A silicon tip on a Nitride lever (with nominal tip radius of 2 nm and a resonance frequency of 70 kHz) was used for all measurements.

Non-resonant Raman spectra were collected using a Labram Aramis (Horiba Jobin-Yvon) equipped with an optical microscope and a 100× objective. A DPSS laser source of 532 nm was used for the excitation of the non-resonant Raman signal that was detected with an an air-cooled CCD. The slit width of the spectrometer was typically set at 100 mm. A diffraction grating with 1800 lines mm^{-1} was used for the collection of all Raman spectra with an overall spectral resolution of ~2 cm^{-1}. Raman spectra have been acquired with an overall acquisition time of 10 s by setting the laser power to 1.40 and 0.02 mW for MoS_2 on Pt and polyimide, respectively.

The electrical characterization of the MoS_2 film (deposited on Pt) was performed at room temperature and in air by current-voltage (I-V) measurements. The curves were carried out using an Imina miBots probe station with Tungsten tips connected to a Keithley 2450 SMU.

3. RESULTS AND DISCUSSION

To study the role of the substrate for MoS_2 thin film formation, the precursor sol (see Figure S1) was spin coated on polyimide, Pt and SiO_2 substrates. The films were annealed in Ar at different temperatures, T = 300°C (polyimide), T = 400°C (Pt and SiO_2) and T = 600/800°C (SiO_2). Chemical analysis of the samples was conducted by X-ray photoelectron spectroscopy (XPS) to investigate the coverage of the substrates and the stoichiometry of the films. XPS survey spectra of films grown on polyimide, Pt and SiO_2 at low temperatures are displayed in Figure 1a.

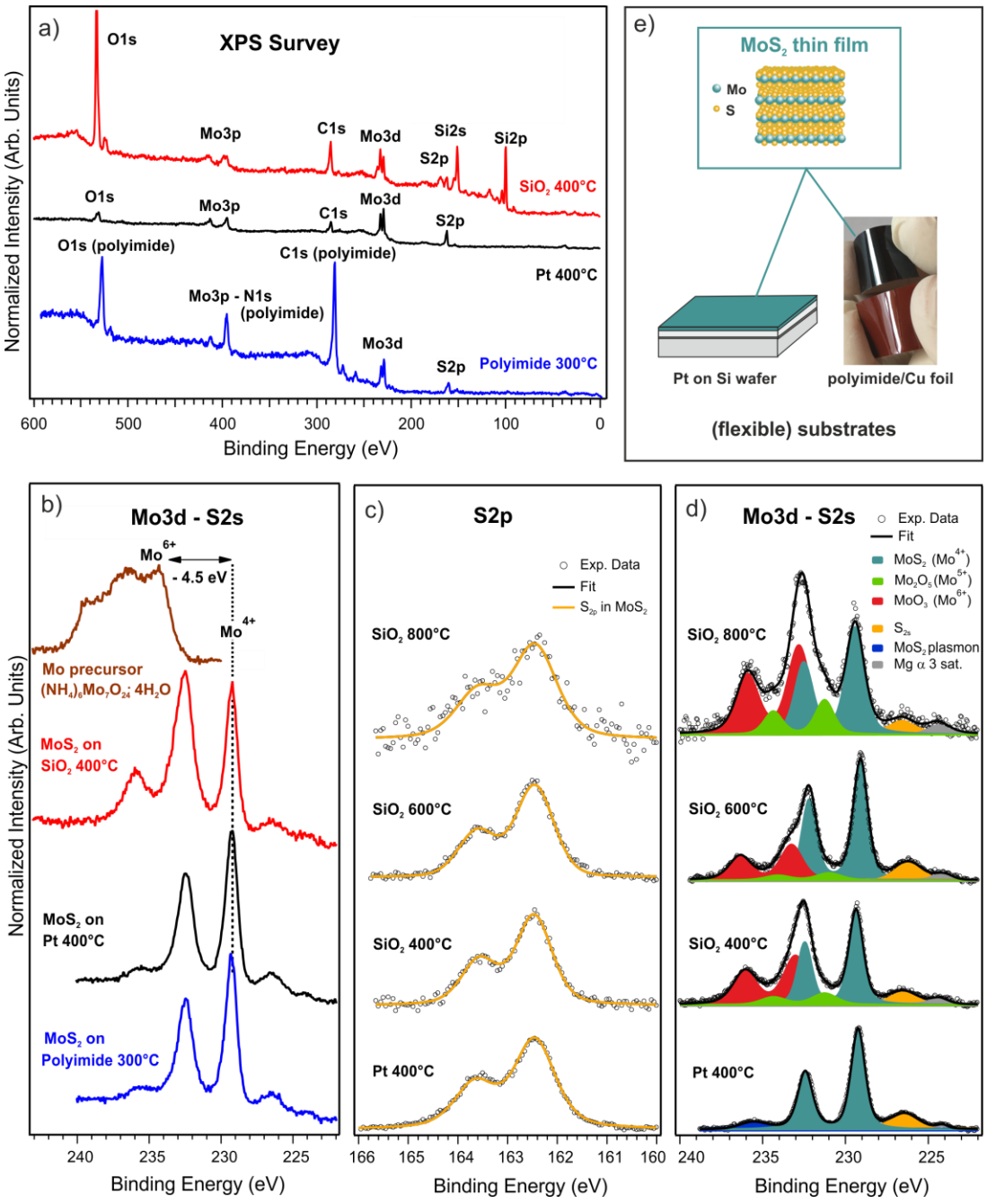

Figure 1. (a) XPS survey spectra of spin coated films on different substrates (polyimide, Pt and SiO_2) annealed at low temperature (T = 300/400°C); (b) Mo 3d + S 2s core level XPS spectra of Mo precursor and spin coated films annealed at low temperature; (c) S 2p and (d) fitted Mo 3d + S 2s core level XPS spectra of spin coated films on Pt and SiO_2 substrates annealed at different temperatures (T = 400 – 800°C); (e) schematic summary of the XPS findings: MoS_2 thin films without any additional oxidized Mo species were formed on Pt and polyimide substrates (upper

substrate in the photograph corresponds to the MoS_2 film on polyimide/Cu foil, whereas the lower one is untreated).

In the MoS_2 film grown on Pt substrate (black curve in Figure 1a), besides Mo, S, and small C- and O-related peaks (i.e., small amount of residual carbon compounds from air contamination) no signal from the Pt (Ti, Si) substrate can be observed, pointing to a good surface wetting and to the formation of large-area continuous MoS_2 layers on Pt. The XPS survey spectrum of the film grown on polyimide (blue curve in Figure 1a), exhibits distinct signals stemming from Mo and S. Moreover, the typical signals from the polyimide layer (i.e., N, C and O) are also detectable, pointing out that the film on polyimide is rather thinner than the one grown on Pt, as expected for a single-step deposition (see section 2.2). Similar to that, the survey spectrum of the film on SiO_2 substantially consist of typical Mo and S peaks together with pronounced intense Si- and O-peaks stemming from the underlying substrate, indicating inhomogeneous coverage of the SiO_2 substrate surface even though a two-step deposition was performed.

In order to follow the Mo^{6+} to Mo^{4+} conversion during film fabrication, we qualitatively compared the Mo 3d core level spectrum of the Mo precursor (powder) with that of the MoS_2 films on the different substrates after annealing at 300°C (polyimide) and 400°C (Pt and SiO_2), see Figure 1b. It can be clearly seen that during film formation Mo^{6+} of the ammonium molybdate precursor is efficiently converted/reduced to Mo^{4+}, that is located at lower binding energies (BEs), corresponding to MoS_2. Furthermore, the samples grown on polyimide and Pt (blue and black curves in Figure 1b) clearly show the two distinct features related to the $Mo3d_{5/2}$ and $Mo3d_{3/2}$ exhibiting the correct splitting spin orbital with the expected energy position of a MoS_2 thin film and a small contribution from MoS_2-related plasmons at higher binding energy, whereas the MoS_2

film on SiO_2 exhibits a minor but distinct peak on the high binding energy side ascribable to the presence of small amount of Mo^{5+} species.

The presence of the above-mentioned component on the MoS_2 film grown on SiO_2 drove us to investigate the effect of both oxidative substrates and high annealing temperatures on sol-gel derived MoS_2 thin film. Figure 1c and d display the S 2p and fitted Mo 3d + S 2s core level spectra of the films grown on SiO_2 and annealed at different temperatures (i.e., 400, 600 and 800°C) compared to the film on Pt (annealed at 400°C). As shown in Figure 1c, the peaks at BEs of 162.5 and 163.6 eV correspond to the S $2p_{3/2}$ and $2p_{1/2}$ core levels. The poor signal-to-noise ratio for the film on SiO_2 annealed at 800°C indicates significant loss of sulfur at high annealing temperatures. This finding is in agreement with the low S/Mo ratio typically reported for film growth at high temperatures, which usually requires additional sulfurization (S precursors) to accomplish highly crystalline and stoichiometric MoS_2 layers.[34,44]

In Figure 1d, the Mo $3d_{5/2}$ and $3d_{3/2}$ peaks stemming from MoS_2 (Mo^{4+} corresponding to gray-blue component) are located at BE = 229.2 and 232.5 eV, respectively, and the S 2s peak (orange component) is observed at BE = 226.4 eV. It can be seen that the film on Pt (annealed at 400°C) only exhibits Mo 3d components from MoS_2. Based on the spectrum, the atomic ratio of S/Mo is 1.85, which is in good agreement with the ratio of 1.92 measured on a MoS_2 single crystal (not shown here). It can be concluded that the annealing process at low temperature (400°C) guarantees an excellent S/Mo ratio on Pt, similar to the one measured on a MoS_2 single crystal.

Different to that, all films on SiO_2 exhibit small amounts of Mo 3d components from higher oxidation states, namely Mo^{5+} and Mo^{6+} (corresponding to green and red component in Figure 1d, respectively) with the Mo $3d_{5/2}$ component located at 231.2 eV and 233.0 eV, respectively, even at low annealing temperature (T = 400 °C). These components can be ascribed to oxidized species

formed during film thermal treatment and become more evident with increasing the annealing temperature. Since the thermal treatment was performed in Ar atmosphere, it can be assumed that the oxygen responsible for the oxidation of Mo^{4+} to Mo^{5+} and Mo^{6+} is provided by the SiO_2 underlying layer. This process becomes more evident at higher annealing temperature (T = 800 °C) where a higher amount of O diffuses into the film. The finding of large-area continuous MoS_2 film formation on non-oxidative substrates, such as Pt and polyimide, is schematically summarized in Figure 1e, where a chemically pure sol-gel derived MoS_2 film is obtained.

It should be noted that different to some other techniques adopted to grow MoS_2 thin films,[31,34,44] no additional S precursor was needed to guarantee an excellent stochiometric S/Mo ratio and to prevent any desulfurization process that would unavoidably affect the MoS_2 chemical properties.

Furthermore, other solution-processed deposition approaches using single-precursor deposition [$(NH_4)_2MoS_4$] on SiO_2 substrates report on the need of special reducing agents[35] or reducing H_2 atmosphere[36,37] to change the oxidation state of Mo^{6+} to Mo^{4+} (MoS_2). We assume that these reducing conditions are always needed to grow MoS_2 on oxide-containing substrates, which act as O source oxidizing the Mo^{4+} to Mo^{5+}/ Mo^{6+} during annealing. However, on non-oxidative substrates, such as Pt and polyimide where the oxygen is not released at annealing temperatures of 400 °C and 300 °C, respectively, strongly reducing conditions are not needed to prevent re-oxidation of the MoS_2 film. Indeed, a recent study[45] using single-precursor deposition and two-step thermal decomposition (at 280/600°C) reports on the synthesis of MoS_2 layers on Ni foil without the need of H_2, supporting our findings that MoS_2 growth on oxide-free substrates can be performed without special means of reducing agents.

The MoS_2 film on Pt substrate was comprehensively characterized with respect to its optical, electronic and structural properties. Spectroscopic ellipsometry (SE) measurements (see details in

Supporting Information) revealed a thickness of about 175 nm, which agrees with a measured thickness of 170 nm via SEM cross-sectional imaging (see Figure S3, Supporting Information).

The electronic properties of the sol-gel derived MoS_2 film on Pt were investigated by UPS and compared to that of an as-received MoS_2 single crystal, see Figure 2a and b. The key physical parameters here are the work function Φ and the position of the valence band maximum (VBM) relative to the Fermi level E_F. The Φ can be calculated by the difference between the energy of the UV photons (21.21 eV for He I radiation used here) and the BE of the SECO. As can be seen in Figure 2a, the SECO positions of sol-gel derived film and single crystal are almost the same, and yield a Φ of 4.25 eV (4.33 eV), which is similar to previous reports.[19,46–48]

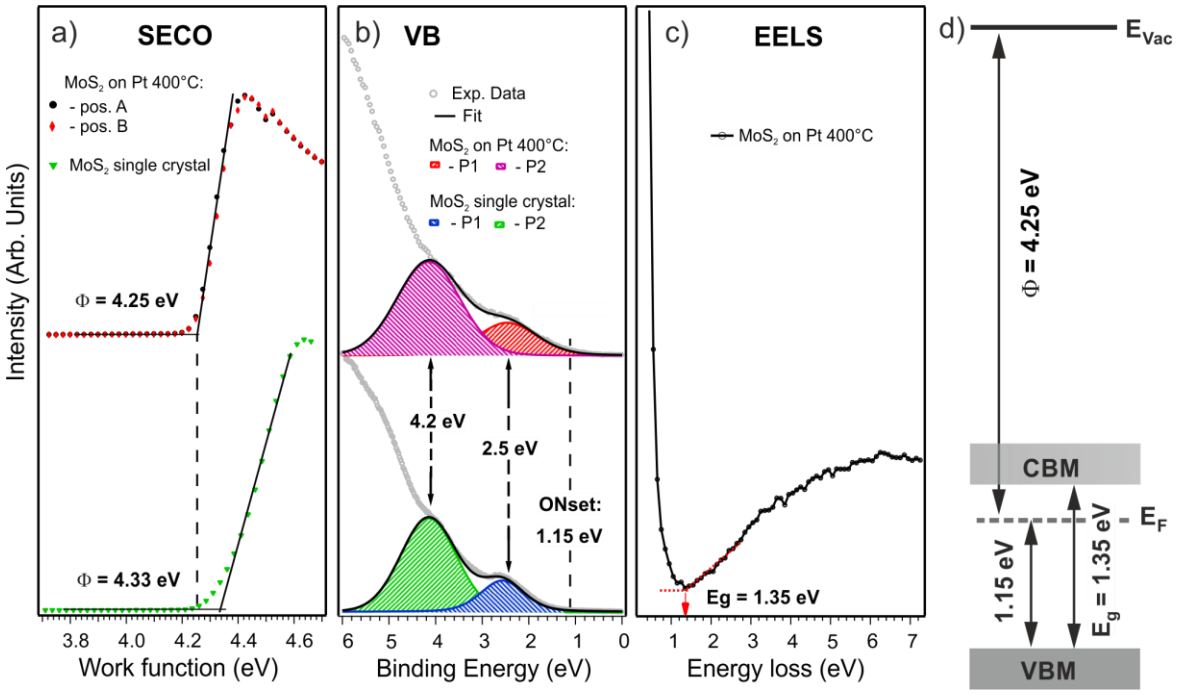

Figure 2. (a) Secondary electron cutoff (SECO) and (b) valence band (VB) region UPS spectra of the sol-gel derived MoS_2 thin film on Pt (annealed in Ar at 400 °C) compared to the spectra of a MoS_2 reference (single crystal); (c) EELS spectrum of the sol-gel derived MoS_2 thin film on Pt; (d) corresponding energy-level diagram. The energetic positions of the Evac and VBM relative to the Fermi level E_F were determined by UPS measurements, whereas the energy gap Eg was derived by EELS.

Furthermore, the valence band of the MoS_2 thin film (upper curve) in Figure 2b exhibits the same profile and structures than the one collected on the single crystal (lower curve). The two features close to E_F can be ascribed to Mo 4d − S 3p hybridized orbitals.[49,50] Furthermore, the VBM of film and single crystal coincides at 1.15 eV, which corresponds to the band structure of a 2H−MoS_2 semiconductor. Fitting analysis of the near E_F region evidences that the two components of both samples have same energy position, full width at half maximum (FWHM) and relative intensity, indicating that the sol-gel derived MoS_2 film on Pt exhibits excellent electronic properties comparable to that of a MoS_2 single crystal. To further investigate the electronic properties of the sol-gel derived MoS_2 thin film, we characterized the band gap E_g of the semiconductor by means of electron energy loss spectroscopy (EELS). The band gap E_g is a crucial value to differentiate the phases of MoS_2 (i.e., semiconducting 2H or metallic 1T phase), and of fundamental importance for any electronic device that implies charge injection or electron-hole recombination between VBM and conduction band minimum (CBM). Figure 2c shows the corresponding EELS spectrum of the sol-gel derived MoS_2 film on Pt, where a MoS_2 band gap E_g of 1.35 eV is observed, in agreement with previous reports for the (indirect) band gap of bulk 2H−MoS_2.[13,14] The band diagram of the fabricated MoS_2 film is reported in Figure 2d. The Fermi level is located in the upper half of the band gap (i.e., 1.15 eV above the VBM), consistently with the n-type nature of the MoS_2.

We further characterized the structural and morphological properties of the sol-gel derived 2H−MoS_2 film on Pt (see Figure 3). The crystal structure was investigated by X-ray diffraction (XRD), as illustrated in Figure 3a.

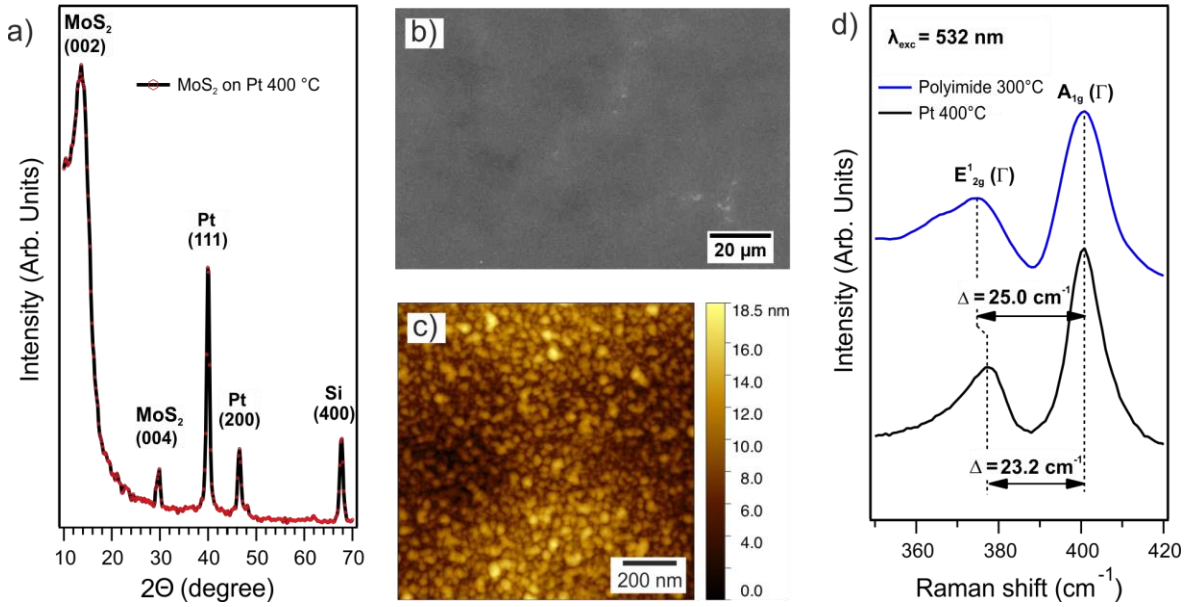

Figure 3. (a) XRD spectrum, (b) SEM image, and c) AFM height image of the sol-gel derived MoS_2 thin film on Pt substrate (annealed in Ar at 400 °C). (d) Non-resonant Raman spectra (λ = 532 nm) of the sol-gel derived MoS_2 thin film on Pt and polyimide substrate. The spectral distance between the $E^1_{2g}(\Gamma)$ and the $A_{1g}(\Gamma)$ Raman modes is given by the vertical dashed lines.

Additional XRD spectra of commercial and sol-gel derived MoS_2 powder annealed at $T = 400°C$ are given in Figure S4 (Supporting Information) indicating a very high crystallinity of sol-gel derived MoS_2 powders even at low-temperature annealing. Furthermore, the XRD spectra in Figure S4 (Supporting Information) helped us in identifying the MoS_2-related peaks in the sol-gel derived thin films. For MoS_2 film on Pt (Figure 3a), two relatively sharp diffraction peaks are observed at 2θ = 13.6° and 29.8° corresponding to the (002) and (004) crystal plane of MoS_2, respectively, whereas the remaining diffraction peaks at 2θ = 40.0°, 46.5 and 67.0° were assigned to crystal planes stemming from the substrate (Pt and Si). It is noteworthy that the (002) peak of the sol-gel derived MoS_2 thin film is slightly shifted to lower angles with respect to the value reported for bulk 2H−MoS_2 (2θ = 14.3° according to PDF no. 37-1492). This shift can be explained with a lattice expansion along the *c*-axis, most probably due to some defect inclusions. This finding

is supported by the value of the interlayer distance calculated via the Bragg equation, which results to be 6.55 Å and is slightly larger than 6.14 Å reported for a standard hexagonal 2H−MoS_2 crystal.[51,52] By applying the Scherrer equation to the (004) peak we determine the average size of the MoS_2 crystallites to be (12 ± 1) nm.

The SEM image of the sample surface in Figure 4b is representative for large sample areas of up to (400 × 400) μm^2, and shows a featureless flat and continuous morphology. The typical AFM height image in Figure 3c reveals the presence of nano-crystallites (root-mean-square roughness of the surface is 2.6 nm) with an average diameter of 15 nm, which agrees with XRD evaluation.

Non-resonant Raman spectra (λ = 532 nm) were collected from the MoS_2 thin films on Pt and polyimide (Figure 3d). Two typical Raman active modes of hexagonal MoS_2 are observed in both samples: E^1_{2g} (in-plane vibrations) at 377.6 cm^{-1} and A_{1g} (out-of-plane vibrations) at 400.8 cm^{-1}. Furthermore, the data reveal typical broadening and phonon shifts with respect to a MoS_2 single crystal as previously observed for MoS_2 thin films grown by different techniques.[53–55] The frequency difference between the E^1_{2g} and A_{1g} Raman modes is ~23.2 cm^{-1} for the MoS_2 thin film on Pt, whereas it is 25 cm^{-1} for the film on polyimide. It is commonly accepted that the spectral distance reflects the number of MoS_2 layers.[56,57] The measured value for the film on polyimide typically corresponds to bulk MoS_2 (25 cm^{-1}), whereas that of the film on Pt lies in between the typical values for bulk and monolayer (18 cm^{-1}). However, our experimentally measured film thickness (see Figure S3, Supporting Information) rules out a few-layered MoS_2 film on Pt, suggesting that the measured value of the spectral distance might also be affected by the lattice strain, as evidenced by the XRD analysis, and by the nature of the underlying substrate.

In order to investigate the electrical properties of sol-gel derived MoS_2 films, and to prove the application of the herein reported deposition technique for electronic applications, the thin film

deposited on Pt was investigated by means of I-V curve measurements (see Figure 4) and in line 4-point-probe sheet resistivity measurements. The inline 4-point probe measurements yielded a sheet resistance in the range from 1.6×10^6 to 1.1×10^6 Ω/sq. Yet due to the fact that there was a certain variation in the film thickness an accurate determination of the value is not possible.

The I-V measurements were carried out in air and at room temperature by contacting the top surface of the MoS_2 film with two tungsten-coated tips of a probe station. Given an average work function of 4.6 eV for the Tungsten, it is expected to form an Ohmic contact between the MoS_2 film and the Tungsten coated tips. The I-V curve of the investigated pristine film is displayed in the semi-log plot in Figure 4a. The solid black line represents a guide for the eye displaying a quadratic relation between current and voltage ($I \sim V^2$). The I-V curve is almost fully symmetric in forward and reverse bias direction and does not exhibit any deviation from the quadratic relation between current and voltage, which is a clear confirmation of an Ohmic contact formed for both carriers. The quadratic relation between current and voltage is typical when the electronic characteristics are determined by space charge limited conductivity (SCLC), which is expected for a trap free material with low carrier density.[58,59] The good agreement between the experimental data and the V^2 dependency indicates that the MoS_2 film deposited has a negligible concentration of shallow trap states above the valence onset (within the gap) as indicated by the UPS measurements in Figure 2b. The very same simple electrical testing configuration was also used to test if the MoS_2 films are being applicable as the active material in resistive random memory devices (ReRAM) as reported before for MoS_2 films fabricated by other techniques.[60–62]

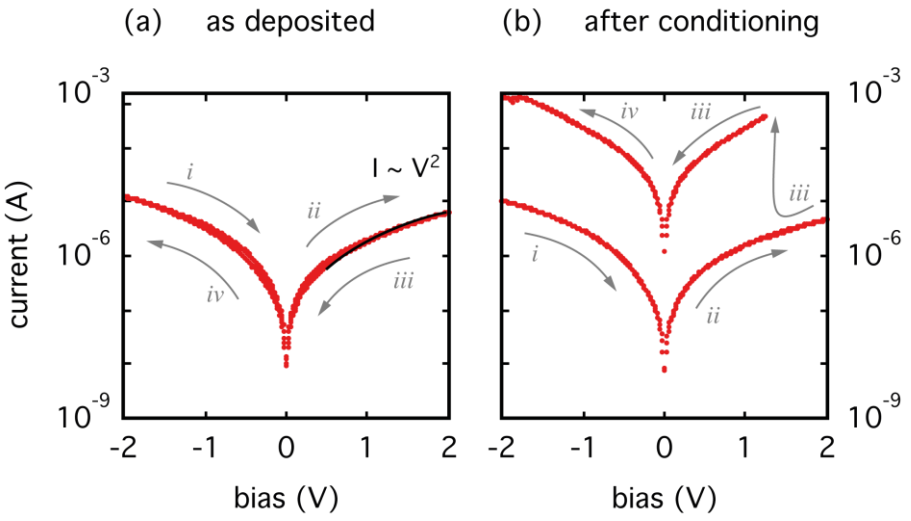

Figure 4. I-V curve measurements performed with a probe station of MoS_2 film grown on Pt. The film was first measured as deposited (a) and then conditioned (b) through sweep cycles (the solid black line represents a guide for the eye indicating a quadratic dependency for I from V). Upon conditioning the film displays a resistive switch from a high to a low state (b). The arrow indicates the voltage sweep progression during I-V measurements.

Upon conditioning (achieved by several forward-reverse bias sweeps at increasing voltage) the MoS_2 film displays abrupt (yet reversible) changes in the film conductivity. The I-V curve in Figure 4b displays the possibility to switch (and thus program via electrical stimuli) the resistivity between a high and a low state with an ON-OFF ratio > 10^2. The resistive switch is achieved upon application of a writing voltage (V_{WRITE} > 1 V). The original low resistivity can be reset to the original state exposing the device to a higher voltage (V_{RESET} > 4 V). This electrical behavior (as well as similar figures of merit such as I-V curve, turn-on bias value and current ratio between the two states) is very similar to what has been already reported for ReRAM based on MoS_2 fabricated by other techniques.[60–62] However, the possibility to solution process MoS_2 and to cure it at low temperature allows the fabrication of memory-based technologies on flexible substrates by means

of low-cost fabrication methods, which will definitely trigger interest in the non-volatile memory community[60–62] and may constitute an true alternative to other organic and hybrid materials currently used in such technologies.[63,64] Furthermore, low temperature solution processed MoS_2 will also find their ways into more complex three-terminal devices such as field effect transistors in a next step.

4. CONCLUSIONS

In the present study, large-area homogeneous thin films of 2H−MoS_2 on technologically relevant substrates were prepared by low-temperature (300°C − 400°C) annealing of a spin coated water-based sol-gel precursor. The role of oxygen-containing substrates, such as SiO_2, in partially re-oxidizing the deposited film (due to oxygen diffusion) was comprehensively studied by XPS. On substrates, where oxygen atoms are not present and/or the oxygen atoms are not released during annealing (e.g. in the case of polyimide), an inert Ar atmosphere was suitable for obtain nanocrystalline 2H−MoS_2 thin films with high spatial homogeneity that show excellent electronic properties for applications in optoelectronic devices. The capability of the sol-gel derived MoS_2 for practical applications in electronic/optoelectronic devices was verified by realizing a resistive random memory device with low erasing and writing voltages threshold. It is expected that the present approach provides a feasible and reliable route for obtaining layer-controlled thin MoS_2 films by tuning the concentration of the sol-gel precursor and the process parameters. Furthermore, it potentially represents a low-cost fabrication method with low environmental impact for large-area coating/printing techniques such as roll-to-roll, blade and spray coating production on metal foils, inkjet printing on flexible polymeric substrates.

ASSOCIATED CONTENT

Supporting Information. Schematic illustration of the molecular structures during sol-gel synthesis (Figure S1). Thermogravimetry and Fourier transform infrared spectroscopy of the (as-precipitated) sol-gel derived MoS_2 powder (Figure S2). Spectroscopic ellipsometry and scanning electron microscopy image of the sol-gel derived MoS_2 film on Pt substrate (Figure S3). X-ray diffraction spectra on commercial and sol-gel derived MoS_2 powder (Figure S4). This material is available free of charge via the Internet at http://pubs.acs.org.

AUTHOR INFORMATION

Corresponding Authors

*marcovittorio.nardi@unitn.it; melanie.timpel@unitn.it

Author Contributions

The manuscript was written through contributions of all authors. All authors have given approval to the final version of the manuscript. Δ These authors contributed equally.

ACKNOWLEDGMENTS

The authors gratefully acknowledge G.D. Sorarù for the thermogravimetric analysis and L. Zottele for his assistance in SEM imaging. We thank L. Lorenzelli for providing the Pt/Ti/Si substrates. M.V.N. and M.T. gratefully acknowledge the support by the CARITRO Foundation (project MILA) Trento (Italy).

REFERENCES

(1) Guo, J.; Wen, R.; Liu, Y.; Zhang, K.; Kou, J.; Zhai, J.; Wang, Z. L. Piezotronic Effect Enhanced Flexible Humidity Sensing of Monolayer MoS_2. *ACS Appl. Mater. Interfaces* **2018**, *10* (9), 8110–8116.

(2) Ganatra, R.; Zhang, Q. Few-Layer MoS_2: A Promising Layered Semiconductor. *ACS Nano* **2014**, *8* (5), 4074–4099.

(3) Theerthagiri, J.; Senthil, R. A.; Senthilkumar, B.; Reddy Polu, A.; Madhavan, J.; Ashokkumar, M. Recent Advances in MoS_2 Nanostructured Materials for Energy and Environmental Applications – A Review. *J. Solid State Chem.* **2017**, *252*, 43–71.

(4) Li, Z.; Meng, X.; Zhang, Z. Recent Development on MoS_2-Based Photocatalysis: A Review. *J. Photochem. Photobiol. C Photochem. Rev.* **2018**, *35*, 39–55.

(5) Bromley, R.; Murray, R. B. The Band Structures of Some Transition Metal Dichalcogenides : I. A Semiempirical Tight Binding Method. *J. Phys. J. Phys. C Solid State Phys* **1972**, *5*, 738–745.

(6) Mattheiss, L. F. Band Structures of Transition-Metal-Dichalcogenide Layer Compounds. *Phys. Rev. B* **1973**, *8* (8), 3719–3740.

(7) Tao, J.; Chai, J.; Lu, X.; Wong, L. M.; Wong, T. I.; Pan, J.; Xiong, Q.; Chi, D.; Wang, S. Growth of Wafer-Scale MoS_2 Monolayer by Magnetron Sputtering. *Nanoscale* **2015**, *7* (6), 2497–2503.

(8) Gustavsson, F.; Svahn, F.; Bexell, U.; Jacobson, S. Nanoparticle Based and Sputtered WS_2

Low-Friction Coatings - Differences and Similarities with Respect to Friction Mechanisms and Tribofilm Formation. *Surf. Coatings Technol.* **2013**, *232*, 616–626.

(9) Topsøe, H.; Clausen, B.; Massoth, F. Hydrotreating Catalysis. In *Catalysis: Science and Technology*; Anderson, J., Boudart, M., Eds.; Springer Berlin Heidelberg: Berlin/Heidelberg, Germany, 1996; pp 1–269.

(10) Sobczynski, A. Molybdenum Disulfide as a Hydrogen Evolution Catalyst for Water Photodecomposition on Semiconductors. *J. Catal.* **1991**, *131* (1), 156–166.

(11) Lin, Y. C.; Dumcenco, D. O.; Huang, Y. S.; Suenaga, K. Atomic Mechanism of the Semiconducting-to-Metallic Phase Transition in Single-Layered MoS_2. *Nat. Nanotechnol.* **2014**, *9* (5), 391–396.

(12) Bronsema, K. D.; De Boer, J. L.; Jellinek, F. On the Structure of Molybdenum Diselenide and Disulfide. *Z. anorg. allg. Chem* **1986**, *540/541*, 15–17.

(13) Mak, K. F.; Lee, C.; Hone, J.; Shan, J.; Heinz, T. F. Atomically Thin MoS_2: A New Direct-Gap Semiconductor. *Phys. Rev. Lett.* **2010**, *105* (13), 136805.

(14) Yu, W. J.; Vu, Q. A.; Oh, H.; Nam, H. G.; Zhou, H.; Cha, S.; Kim, J.-Y.; Carvalho, A.; Jeong, M.; Choi, H.; et al. Unusually Efficient Photocurrent Extraction by Tunnelling through Discretized Barriers. *Nat. Commun.* **2016**, *7*, 13278.

(15) Park, S.; Mutz, N.; Schultz, T.; Blumstengel, S.; Han, A.; Aljarb, A.; Li, L.-J.; List-Kratochvil, E. J. W.; Amsalem, P.; Koch, N. Direct Determination of Monolayer MoS_2 and WSe_2 Exciton Binding Energies on Insulating and Metallic Substrates. *2D Mater.* **2018**, *5*

(2), 025003.

(16) Radisavljevic, B.; Radenovic, A.; Brivio, J.; Giacometti, V.; Kis, A. Single-Layer MoS_2 Transistors. *Nat. Nanotechnol.* **2011**, *6* (3), 147–150.

(17) Huo, N.; Yang, S.; Wei, Z.; Li, S.-S.; Xia, J.-B.; Li, J. Photoresponsive and Gas Sensing Field-Effect Transistors Based on Multilayer WS_2 Nanoflakes. *Sci. Rep.* **2014**, *4*, 5209.

(18) Yin, Z.; Li, H.; Li, H.; Jiang, L.; Shi, Y.; Sun, Y.; Lu, G.; Zhang, Q.; Chen, X.; Zhang, H. Single-Layer MoS_2 Phototransistors. *ACS Nano* **2012**, *6* (1), 74–80.

(19) Gobbi, M.; Bonacchi, S.; Lian, J. X.; Bertolazzi, A. V. S.; Zyska, B.; Timpel, M.; Tatti, R.; Olivier, Y.; Hecht, S.; Nardi, M. V.; et al. Collective Molecular Switching in Hybrid Superlattices for Light-Modulated Two-Dimensional Electronics. *Nat. Commun.* **2018**, *9*, 2661.

(20) Zhu, Y.; Li, Y.; Arefe, G.; Burke, R. A.; Tan, C.; Hao, Y.; Liu, X.; Liu, X.; Yoo, W. J.; Dubey, M.; et al. Monolayer Molybdenum Disulfide Transistors with Single-Atom-Thick Gates. *Nano Lett.* **2018**, *18*, 3807–3813.

(21) Jaegermann, W.; Tributsch, H. Interfacial Properties of Semiconducting Transition Metal Chalcogenides. *Prog. Surf. Sci.* **1988**, *29* (1–2), 1–167.

(22) Benck, J. D.; Hellstern, T. R.; Kibsgaard, J.; Chakthranont, P.; Jaramillo, T. F. Catalyzing the Hydrogen Evolution Reaction (HER) with Molybdenum Sulfide Nanomaterials. *ACS Catal.* **2014**, *4* (11), 3957–3971.

(23) Stephenson, T.; Li, Z.; Olsen, B.; Mitlin, D. Lithium Ion Battery Applications of

Molybdenum Disulfide (MoS_2) Nanocomposites. *Energy Environ. Sci.* **2014**, *7* (1), 209–231.

(24) Gao, M. R.; Xu, Y. F.; Jiang, J.; Yu, S. H. Nanostructured Metal Chalcogenides: Synthesis, Modification, and Applications in Energy Conversion and Storage Devices. *Chem. Soc. Rev.* **2013**, *42* (7), 2986–3017.

(25) Huang, X.; Zeng, Z.; Zhang, H. Metal Dichalcogenide Nanosheets: Preparation, Properties and Applications. *Chem. Soc. Rev.* **2013**, *42* (5), 1934–1946.

(26) Xu, B.; Cheng, Y.; Wang, Y.; Huang, Y.; Peng, J.; Luo, Z.; Xu, H.; Cai, Z.; Weng, J.; Moncorgé, R. Passively Q-Switched Nd:$YAlO_3$ Nanosecond Laser Using MoS_2 as Saturable Absorber. *Opt. Express* **2014**, *22* (23), 28934–28940.

(27) Voiry, D.; Yamaguchi, H.; Li, J.; Silva, R.; Alves, D. C. B.; Fujita, T.; Chen, M.; Asefa, T.; Shenoy, V. B.; Eda, G.; et al. Enhanced Catalytic Activity in Strained Chemically Exfoliated WS_2 Nanosheets for Hydrogen Evolution. *Nat. Mater.* **2013**, *12* (9), 850–855.

(28) Liu, N.; Baek, J.; Kim, S. M.; Hong, S.; Hong, Y. K.; Kim, Y. S.; Kim, H.-S.; Kim, S.; Park, J. Improving the Stability of High-Performance Multilayer MoS_2 Field-Effect Transistors. *ACS Appl. Mater. Interfaces* **2017**, *9*, 42943−42950.

(29) Dumcenco, D.; Ovchinnikov, D.; Marinov, K.; Lazić, P.; Gibertini, M.; Marzari, N.; Sanchez, O. L.; Kung, Y. C.; Krasnozhon, D.; Chen, M. W.; et al. Large-Area Epitaxial Monolayer MoS_2. *ACS Nano* **2015**, *9* (4), 4611–4620.

(30) Lee, J.; Pak, S.; Giraud, P.; Lee, Y.; Cho, Y.; Hong, J.; Jang, A.; Chung, H.; Hong, W.;

Jeong, H. Y.; et al. Thermodynamically Stable Synthesis of Large-Scale and Highly Crystalline Transition Metal Dichalcogenide Monolayers and Their Unipolar N–n Heterojunction Devices. *Adv. Mater.* **2017**, *29*, 1702206.

(31) Zheng, W.; Lin, J.; Feng, W.; Xiao, K.; Qiu, Y.; Chen, X. S.; Liu, G.; Cao, W.; Pantelides, S. T.; Zhou, W.; et al. Patterned Growth of P-Type MoS_2 Atomic Layers Using Sol-Gel as Precursor. *Adv. Funct. Mater.* **2016**, *26* (35), 6371–6379.

(32) Pütz, J.; Aegerter, M. A. Spin Deposition of MoS_x Thin Films. *Thin Solid Films* **1999**, *351*, 119–124.

(33) George, A. S.; Mutlu, Z.; Ionescu, R.; Wu, R. J.; Jeong, J. S.; Bay, H. H.; Chai, Y.; Mkhoyan, K. A.; Ozkan, M.; Ozkan, C. S. Wafer Scale Synthesis and High Resolution Structural Characterization of Atomically Thin MoS_2 Layers. *Adv. Funct. Mater.* **2014**, *24* (47), 7461–7466.

(34) Kwon, K. C.; Kim, C.; Le, Q. Van; Gim, S.; Jeon, J. M.; Ham, J. Y.; Lee, J. L.; Jang, H. W.; Kim, S. Y. Synthesis of Atomically Thin Transition Metal Disulfides for Charge Transport Layers in Optoelectronic Devices. *ACS Nano* **2015**, *9* (4), 4146–4155.

(35) Xi, Y.; Serna, M. I.; Cheng, L.; Gao, Y.; Baniasadi, M.; Rodriguez-Davila, R.; Kim, J.; Quevedo-Lopez, M. A.; Minary-Jolandan, M. Fabrication of MoS_2 Thin Film Transistors via Selective-Area Solution Deposition Methods. *J. Mater. Chem. C* **2015**, *3* (16), 3842–3847.

(36) Lim, Y. R.; Song, W.; Han, J. K.; Lee, Y. B.; Kim, S. J.; Myung, S.; Lee, S. S.; An, K. S.; Choi, C. J.; Lim, J. Wafer-Scale, Homogeneous MoS_2 Layers on Plastic Substrates for

Flexible Visible-Light Photodetectors. *Adv. Mater.* **2016**, *28*, 5025–5030.

(37) Yang, H.; Giri, A.; Moon, S.; Shin, S.; Myoung, J. M.; Jeong, U. Highly Scalable Synthesis of MoS_2 Thin Films with Precise Thickness Control via Polymer-Assisted Deposition. *Chem. Mater.* **2017**, *29* (14), 5772–5776.

(38) Ionescu, R.; Campbell, B.; Wu, R.; Aytan, E.; Patalano, A.; Ruiz, I.; Howell, S. W.; McDonald, A. E.; Beechem, T. E.; Mkhoyan, K. A.; et al. Chelant Enhanced Solution Processing for Wafer Scale Synthesis of Transition Metal Dichalcogenide Thin Films. *Sci. Rep.* **2017**, *7* (1), 6419.

(39) Sahatiya, P.; Jones, S. S.; Badhulika, S. Direct, Large Area Growth of Few-Layered MoS2 Nanostructures on Various Flexible Substrates: Growth Kinetics and Its Effect on Photodetection Studies. *Flex. Print. Electron.* **2018**, *3*, 015002.

(40) Panigrahi, P. K.; Pathak, A. Aqueous Medium Synthesis Route for Randomly Stacked Molybdenum Disulfide. *J. Nanoparticles* **2013**, *671214*, 1–10.

(41) Guo, X.; Wang, Z.; Zhu, W.; Yang, H. The Novel and Facile Preparation of Multilayer MoS_2 Crystals by a Chelation-Assisted Sol–gel Method and Their Electrochemical Performance. *RSC Adv.* **2017**, *7*, 9009–9014.

(42) Prusakova, V.; Armellini, C.; Carpentiero, A.; Chiappini, A.; Collini, C.; Dirè, S.; Ferrari, M.; Lorenzelli, L.; Nardello, M.; Normani, S.; et al. Morphologic, Structural, and Optical Characterization of Sol-Gel Derived TiO_2 Thin Films for Memristive Devices. *Phys. Status Solidi* **2015**, *12*, 192–196.

(43) Prusakova, V.; Collini, C.; Nardi, M.; Tatti, R.; Lunelli, L.; Vanzetti, L.; Lorenzelli, L.; Baldi, G.; Chiappini, A.; Chiasera, A.; et al. The Development of Sol–gel Derived TiO_2 Thin Films and Corresponding Memristor Architectures. *RSC Adv.* **2017**, *7* (3), 1654–1663.

(44) Liu, K. K.; Zhang, W.; Lee, Y. H.; Lin, Y. C.; Chang, M. T.; Su, C. Y.; Chang, C. S.; Li, H.; Shi, Y.; Zhang, H.; et al. Growth of Large-Area and Highly Crystalline MoS_2 Thin Layers on Insulating Substrates. *Nano Lett.* **2012**, *12* (3), 1538–1544.

(45) Lim, Y. R.; Han, J. K.; Kim, S. K.; Lee, Y. B.; Yoon, Y.; Kim, S. J.; Min, B. K.; Kim, Y.; Jeon, C.; Won, S.; et al. Roll-to-Roll Production of Layer-Controlled Molybdenum Disulfide: A Platform for 2D Semiconductor-Based Industrial Applications. *Adv. Mater.* **2018**, *30* (5), 1–8.

(46) Yun, J.-M.; Noh, Y.-J.; Yeo, J.-S.; Go, Y.-J.; Na, S.-I.; Jeong, H.-G.; Kim, J.; Lee, S.; Kim, S.-S.; Koo, H. Y.; et al. Efficient Work-Function Engineering of Solution-Processed MoS_2 Thin-Films for Novel Hole and Electron Transport Layers Leading to High-Performance Polymer Solar Cells. *J. Mater. Chem. C* **2013**, *1* (24), 3777–3783.

(47) Qin, P.; Fang, G.; Ke, W.; Cheng, F.; Zheng, Q.; Wan, J.; Lei, H.; Zhao, X. In Situ Growth of Double-Layer MoO_3/MoS_2 Film from MoS_2 for Hole-Transport Layers in Organic Solar Cell. *J. Mater. Chem. A* **2014**, *2* (8), 2742–2756.

(48) Jiao, K.; Duan, C.; Wu, X.; Chen, J.; Wang, Y.; Chen, Y. The Role of MoS_2 as an Interfacial Layer in Graphene/Silicon Solar Cells. *Phys. Chem. Chem. Phys.* **2015**, *17* (12), 8182–8186.

(49) Lu, S.-C.; Leburton, J.-P. Electronic Structures of Defects and Magnetic Impurities in MoS_2 Monolayers. *Nanoscale Res. Lett.* **2014**, *9* (1), 676.

(50) Ahmad, S.; Mukherjee, S. A Comparative Study of Electronic Properties of Bulk MoS_2 and Its Monolayer Using DFT Technique: Application of Mechanical Strain on MoS_2 Monolayer. *Graphene* **2014**, *03* (04), 52–59.

(51) Fan, X.; Khosravi, F.; Rahneshin, V.; Shanmugam, M.; Loeian, M.; Jasinski, J.; Cohn, R. W.; Terentjev, E.; Panchapakesan, B. MoS_2 Actuators: Reversible Mechanical Responses of MoS_2-Polymer Nanocomposites to Photons. *Nanotechnology* **2015**, *26*, 261001.

(52) Fan, X.; Xu, P.; Zhou, D.; Sun, Y.; Li, Y. C.; Nguyen, M. A. T.; Terrones, M.; Mallouk, T. E. Fast and Efficient Preparation of Exfoliated 2H MoS_2 Nanosheets by Sonication-Assisted Lithium Intercalation and Infrared Laser-Induced 1T to 2H Phase Reversion. *Nano Lett.* **2015**, *15* (9), 5956–5960.

(53) Late, D. J.; Shaikh, P. A.; Khare, R.; Kashid, R. V.; Chaudhary, M.; More, M. A.; Ogale, S. B. Pulsed Laser-Deposited MoS_2 Thin Films on W and Si: Field Emission and Photoresponse Studies. *ACS Appl. Mater. Interfaces* **2014**, *6* (18), 15881–15888.

(54) Shinde, S. M.; Kalita, G.; Tanemura, M. Fabrication of Poly(Methyl Methacrylate)-MoS_2/Graphene Heterostructure for Memory Device Application. *J. Appl. Phys.* **2014**, *116* (21), 214306.

(55) Kong, D.; Wang, H.; Cha, J. J.; Pasta, M.; Koski, K. J.; Yao, J.; Cui, Y. Synthesis of MoS_2 and $MoSe_2$ Films with Vertically Aligned Layers. *Nano Lett.* **2013**, *13* (3), 1341–1347.

(56) Li, H.; Zhang, Q.; Yap, C. C. R.; Tay, B. K.; Edwin, T. H. T.; Olivier, A.; Baillargeat, D. From Bulk to Monolayer MoS_2: Evolution of Raman Scattering. *Adv. Funct. Mater.* **2012**, *22* (7), 1385–1390.

(57) Ottaviano, L.; Palleschi, S.; Perrozzi, F.; D'Olimpio, G.; Priante, F.; Donarelli, M.; Benassi, P.; Nardone, M.; Gonchigsuren, M.; Gombosuren, M.; et al. Mechanical Exfoliation and Layer Number Identification of MoS_2 Revisited. *2D Mater.* **2017**, *4* (4), 045013.

(58) Frank, R. I.; Simmons, J. G. Space-Charge Effects on Emission-Limited Current Flow in Insulators. *J. Appl. Phys.* **1967**, *38* (2), 832–840.

(59) Ghatak, S.; Ghosh, A. Observation of Trap-Assisted Space Charge Limited Conductivity in Short Channel MoS_2 Transistor. *Appl. Phys. Lett.* **2013**, *103* (12), 122103.

(60) Yin, Z.; Zeng, Z.; Liu, J.; He, Q.; Chen, P.; Zhang, H. Memory Devices Using a Mixture of MoS_2 and Graphene Oxide as the Active Layer. *Small* **2013**, *9* (5), 727–731.

(61) Wang, W.; Panin, G. N.; Fu, X.; Zhang, L.; Ilanchezhiyan, P. MoS_2 Memristor with Photoresistive Switching. *Sci. Rep.* **2016**, *6*, 31224.

(62) Cheng, P.; Sun, K.; Hu, Y. H. Memristive Behavior and Ideal Memristor of 1T Phase MoS_2 Nanosheets. *Nano Lett.* **2016**, *16* (1), 572–576.

(63) Nau, S.; Wolf, C.; Popovic, K.; Blümel, A.; Santoni, F.; Gagliardi, A.; di Carlo, A.; Sax, S.; List-Kratochvil, E. J. W. Inkjet-Printed Resistive Switching Memory Based on Organic Dielectric Materials: From Single Elements to Array Technology. *Adv. Electron. Mater.* **2015**, *1* (1–2), 1400003.

(64) Nau, S.; Sax, S.; List-Kratochvil, E. J. W. Unravelling the Nature of Unipolar Resistance Switching in Organic Devices by Utilizing the Photovoltaic Effect. *Adv. Mater.* **2014**, *26* (16), 2508–2513.

Insert Table of Contents Graphic and Synopsis Here